ACS OMEGA

Open Access

http://pubs.acs.org/journal/acsodf

Article

Defect-Driven MoS_2 Nanosheets toward Enhanced Sensing Sensitivity

Ly Tan Nhiem, Do Thuy Khanh Linh, Hang Nguyen, and Nguyen Huu Hieu*

Cite This: *ACS Omega* 2024, 9, 27065−27070

Read Online

ACCESS | Metrics & More | Article Recommendations | Supporting Information

ABSTRACT: In this study, S-deficient MoS_2 was prepared using proton irradiation and then applied as sensing materials for the detection of NO_2 gas. First, bulk MoS_2 was treated by ultrasonics to produce 2D nanosheets of MoS_2, which were subsequently bombarded by a flux of high-energy protons, resulting in the appearance of structural defects throughout MoS_2. The proton fluxes were adjusted to different densities of 1×10^{11}, 1×10^{12}, 1×10^{13}, and 1×10^{14} ions/cm^2. The effects of proton irradiation on the defects, also referred to as atomic vacancies, were systematically investigated using Raman measurements to locate the E^1_{2g} and A_{1g} modes and X-ray photoelectron spectroscopy to determine the binding energy of Mo 3d and S 2p orbitals. It was revealed that the density of proton irradiation greatly affects the degree of S atom vacancies in irradiated MoS_2, while also enhancing the n-type semiconducting behaviors of MoS_2. The vacancy-rich MoS_2 was then demonstrated to exhibit a higher response to NO_2 gas compared to that of nonirradiated MoS_2, showing a 4-fold increase in response within a concentration range from 1 to 20 ppm. These results could pave the way for new approaches to fabricating sensing materials.

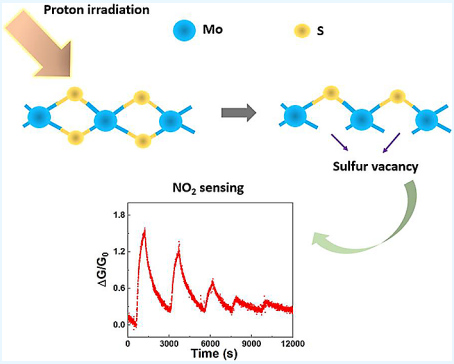

1. INTRODUCTION

Recently, molybdenum disulfide (MoS_2) has emerged as one of the most studied transition metal dichalcogenide materials due to its versatile properties, which can be utilized as metals,[1] semi-metals, semiconductors, and even superconductors.[2] Bulk MoS_2 is known to consist of 2D crystal layers, with one plane of hexagonally arranged molybdenum sandwiched between two planes of sulfur atoms, resulting in a trigonal prismatic arrangement of S−Mo−S covalently bonded atoms.[3] Through nanofabrication techniques, bulk MoS2 can be broken down into separate 2D layers with thicknesses of several nanometers or deliberately shaped into various morphologies.[4] Such nanostructures have been demonstrated to exhibit superior characteristics in a wide range of applications, including sensing,[5] photovoltaics,[6] energy storage,[7] catalysis,[8] and more.

In gas sensing, several approaches have been applied to utilize MoS_2 as a recognition interface.[9] For example, MoS_2 flakes were successfully incorporated into field-effect transistor-based gas sensors for detecting NO_2[10] and NH_3.[11] The sensing sensitivity of the MoS_2-based sensor can be considered comparable to that of other nanomaterials such as graphene,[12,13] nanoparticles,[14] and nanocomposites.[15−17] To enhance sensing sensitivity, chemical-vapor-deposition-grown MoS_2 was employed.[18] Instead of MoS_2 flakes, the monolayer of MoS_2 exhibited outstanding sensitivity with a detection limit as low as 20 ppb for NO_2 and 1 ppm for NH_3 at room temperature. Alternatively, hierarchical hollow spheres of MoS_2 were fabricated to improve the exposure of active edge sites of MoS_2 compared to smooth solid structures, significantly enhancing sensing performance toward NO_2 gas.[19] Moreover, MoS_2 was integrated with sensing materials to achieve synergistic effects in resulting composites, such as single-walled carbon nanotube/MoS_2,[20] graphene/MoS_2,[21] polyaniline/MoS_2,[22] Au nanoparticles/MoS_2,[23] and more.

To date, it has been known that the electronic structures of MoS_2 can be altered by high-energy proton irradiation.[24,25] The irradiated MoS_2 showed a significant decrease in work function, and the Fermi level shifted due to atomic vacancies, which is expected to greatly enhance sensing capabilities. However, there have been few studies investigating the correlation between the sensing sensitivity of MoS_2 and proton irradiation. Considering that this approach is of great importance for enhancing the sensitivity of MoS2 at the molecular level, in this study, we prepared MoS_2 nanosheets that were then subjected to proton irradiation. NO_2 gas sensing was conducted with the corresponding irradiated MoS_2, and the electronic states of MoS_2 were carefully monitored using Raman and X-ray photoelectron microscopy.

Received: January 11, 2024
Revised: May 31, 2024
Accepted: June 7, 2024
Published: June 13, 2024

2. EXPERIMENTAL SECTION

2.1. Fabrication of MoS_2 Nanosheets. Bulk MoS_2 (Crystal, 99.995%) (300 mg) was dispersed in 150 mL of 1% solution of sodium dodecyl sulfate (SDS, ACS reagent, ≥99.0%) using an ultrasonic processor (Branson SFX150) with a power of 150 W in 8 h. The resulting dispersion was then centrifuged at 7000 rpm for 30 min to collect residues. The products were thoroughly washed with ethanol (absolute, 99,99%) and acetone (ACS reagent, ≥99.5%) and dried in ambient conditions. Deionized (DI) water (18.2 MΩ cm) was used in all the experiments.

2.2. Proton Irradiation of MoS_2 Nanosheets. An MC-50 cyclotron was utilized to subject MoS_2 nanosheets to proton irradiation at the Korea Institute of Radiological and Medical Sciences (KIRAMS). The proton beam was set to maintain a constant energy flux of 10 MeV, and the duration of irradiation was adjusted to produce proton beam fluxes with different densities of 1×10^{11}, 1×10^{12}, 1×10^{13}, and 1×10^{14} ions/cm^2. All experiments were conducted at room temperature. The irradiated MoS_2 nanosheets were obtained in the powder form.

2.3. Fabrication of Sensor Devices. Interdigitated microelectrodes (IDEs, J-solution), consisting of pairs of gold electrodes deposited on a SiO_2 wafer, were used as the substrate for the deposition of MoS_2 nanosheets. The IDEs were initially cleaned with acetone and DI water through sonication for 30 min and subsequently dried at 60 °C. The MoS_2, dispersed in acetone at a concentration of 4 mg/mL, was coated onto the IDEs using drop-casting. The resulting MoS_2-deposited IDEs were then dried at 80 °C and stored in a vacuum prior to use.

2.4. Characterization and Sensing. For materials characterization, atomic-force microscopy (AFM) (N8-MEPS. Bruker) and field emission scanning electron microscopy (FE-SEM, JSM-7100F; JEOL) were employed to unveil the surface morphology and thickness of MoS_2 nanosheets. Raman spectroscopy (RA-TN05, 532 nm, Horiba Scientific) and X-ray photoelectron spectroscopy (XPS, K-alpha; Thermo Scientific Inc.) were utilized to monitor the changes in the electronic vibrations and chemical structures of MoS_2 under various irradiation conditions.

2.5. Gas Sensing Experiment. A gas chamber (P7000; Made Lab), equipped with a computer-interfaced multichannel source meter (2400, Keithley), and mass flow controllers (MFC, MPR-3000S, MFC Korea), was used to conduct the sensing experiment. The MoS_2-deposited IDEs were initially placed in an environment filled with carrier gas N_2 at 1 atm. They were then exposed to NO_2 gas, which was well-diluted in a stream of N_2 at different concentrations. For consecutive sensing tests, the chamber was evacuated by flowing a stream of N_2, followed by the injection of appropriate amounts of the target gas, NO_2. The sensing signal was monitored in real-time by the source meter, observing the resistance change of the MoS_2 nanosheets upon exposure to NO_2.

3. RESULTS AND DISCUSSION

The bulk MoS_2 was used as precursors in the preparation of MoS_2 nanosheets, as mentioned above. The interaction between the MoS_2 sheets and the anionic surfactant SDS is critical for the formation of the nanosheets.[26] As indicated in Figure 1a,b, it is clearly shown that the large MoS_2 clusters were exfoliated into smaller MoS_2 flakes, which were quite uniform in size and shape. Further examination was conducted by using AFM, as shown in Figure 1c. The results showed that the thickness of exfoliated MoS_2 was approximately 4 nm, which can be estimated to consist of 6 layers of 2D crystal MoS_2, with 0.65 nm for each layer.[27] The SDS molecules are known to exhibit strong electrostatic interactions with the surface of the MoS_2 sheets. Randomly arranged monolayers of SDS molecules on the surfaces act as passivating layers to prevent the exfoliated MoS_2 from aggregating.[26]

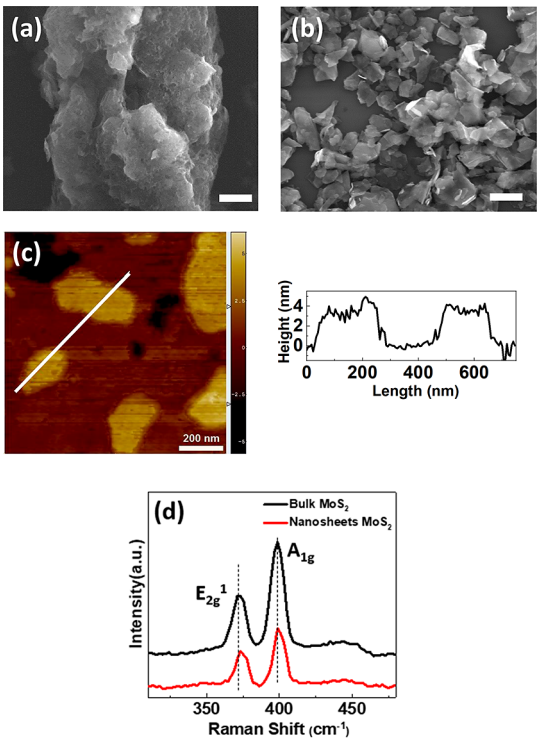

Figure 1. SEM image of (a) Bulk MoS_2; (b) exfoliated nanosheets of MoS_2; (c) AFM and height profile of MoS_2 nanosheets; and (d) Raman spectra of bulk MoS_2 and exfoliated MoS_2. The scale bar is 200 nm.

Importantly, Raman spectroscopy was also conducted to examine both the bulk and exfoliated MoS_2 (Figure 1d). It was observed that there are two characteristic peaks of MoS_2 corresponding to the in-plane vibration of two S atoms with respect to the Mo atom (E^1_{2g} peak) and the out-of-plane vibration of S atoms in opposite directions (A_{1g} peak).[27] One can see that the exfoliated MoS_2 still exhibited vibration peaks at corresponding positions compared to those of the precursors. This strongly suggests that the chemical structures of exfoliated MoS_2 were not damaged by ultrasonics. The A_{1g} mode is known to be very sensitive to the deposition and/or removal of elements on the MoS_2 outer surface.[28] Even a tiny addition could trigger significant shifts in vibration modes, making it easily monitored by Raman spectroscopy.[29] Taking this into account, proton irradiation was conducted on the exfoliated MoS_2 with different densities of 10^{11}, 10^{12}, 10^{13}, and 10^{14} ions/cm^2, along with nonirradiated MoS_2 for comparison. The MoS_2 materials were denoted as i10^{11}, i10^{12}, i10^{13}, and i10^{14}, respectively.

As shown in Figure 2, all the samples exhibited characteristic Raman spectra, and an obvious redshift was observed, which was correlated with the density of proton irradiation, this trend was in consistent with previous studies.[25,30] Both vibration

https://doi.org/10.1021/acsomega.4c00379
ACS Omega 2024, 9, 27065−27070

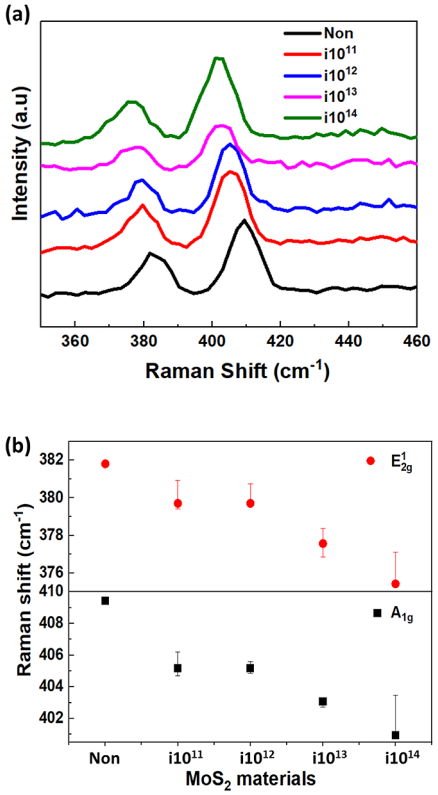

Figure 2. (a) Raman spectra of the exfoliated MoS_2 materials with different densities of irradiation; (b) dependency of Raman shifts on irradiation density.

modes were shifted to lower wavenumbers, corresponding to longer wavelengths of the vibrations. In E^1_{2g} modes, Raman shifts were observed from 382 to 379 cm^{-1} for the nonirradiated and $i10^{14}$ samples, respectively. Meanwhile, a shift from 409 to 401 cm^{-1} was recorded for A_{1g} modes. The higher the irradiation density, the larger the Raman shifts obtained. In the ordinary states of MoS_2, the interlayer van der Waals forces suppress atom vibrations, resulting in A_{1g} and E^1_{2g} modes at specific wavenumbers for a given type of MoS_2.[29] After proton irradiation, however, the S atoms were observed to vibrate more freely in both the out-of-plane and in-plane modes. This was presumably due to the impact of proton interaction; a portion of S atoms were removed from the 2D layer of MoS_2, providing the remaining S atoms with more space to vibrate and reducing repulsion interactions. These S vacancies ultimately led to vibrations with longer wavelengths, as monitored above, and were assumed to be proportionally dependent on proton irradiation.

To clarify the structural changes of irradiated MoS_2, further examination of the samples was conducted with XPS measurements. Spectra of binding energies (BE) related to valence orbitals in MoS_2 materials were depicted, and deconvolution was also performed to distinguish these states as shown in Figure 3. All the samples exhibited characteristic BE relating to Mo $3d_{3/2}$, Mo $3d_{5/2}$, S 2s, and S $2p_{3/2}$ orbitals.[31] Importantly, the dominant Mo $3d_{5/2}$ and S $2p_{3/2}$ doublets were found to be around 233 and 162.5 eV. These doublets could be deconvoluted into smaller doublets, revealing a portion of the nonstoichiometric Mo_xS_y with oxidation states that exist alongside MoS_2. There are two types of sulfur atom vacancies in MoS_2. Through the analysis of scanning tunneling microscopy (STM) images and density functional theory (DFT) calculations, it has been determined that disulfur vacancies occur at significantly lower concentrations compared to vacancies involving single sulfur atoms. This phenomenon leads to the formation of Mo_xS_y compounds.[32] It is known that the Mo_xS_y, coexisting with MoS_2, makes the overall stoichiometry appear to be 1.8:1 (S/Mo), rather than 2:1.[33]

As shown in Figure 3a, the proportion of Mo_xS_y was found to increase with the density of proton irradiation in this study, which led to a decrease in the overall stoichiometric ratio between S and Mo atoms.[34] In other words, the amount of S

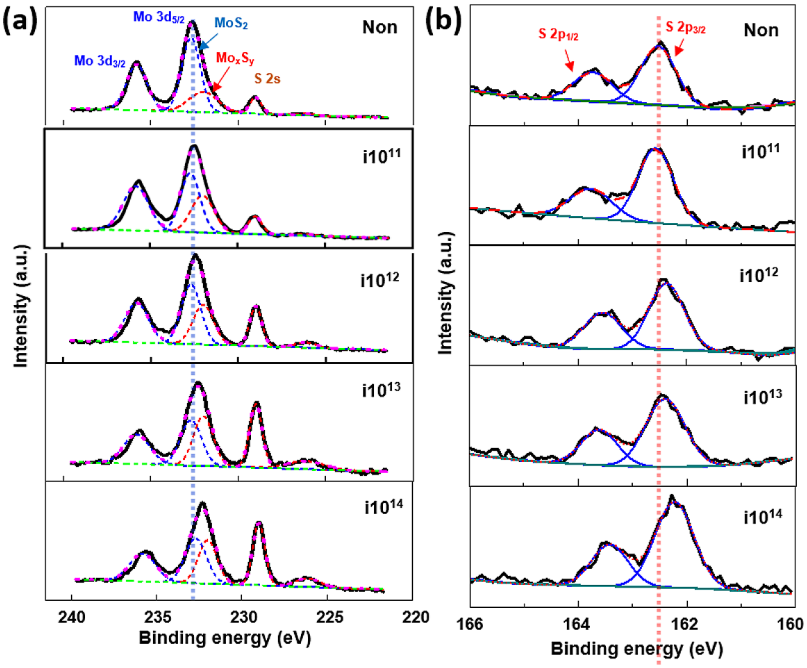

Figure 3. XPS spectra of the exfoliated MoS_2 materials at (a) Mo 3d orbitals and (b) S 2p orbitals.

https://doi.org/10.1021/acsomega.4c00379
ACS Omega 2024, 9, 27065−27070

vacancies increased with proton irradiation, and native S vacancies that existed in MoS_2 materials before proton irradiation were enlarged under the impact of the proton beam. This result was consistent with the Raman shifts discussed above and supported by other studies.[34,35] MoS_2 materials are known to exhibit n-type semiconducting behavior due to intrinsic S vacancies.[36] In the MoS_2 configuration, the Mo $3d_{5/2}$ orbitals are responsible for forming Mo−S bonds, while the Mo $3d_{3/2}$ orbitals and S 2p orbitals are free above the surface of the MoS_2 plane.[9] When the S vacancies occur, the Mo $3d_{5/2}$ orbitals are left negatively charged, ultimately enhancing the n-type behavior of the resulting MoS_2.[9] Overall, the S vacancies and concomitant n-type doping were greatly dependent on proton irradiation. Such a negatively charged surface of irradiated MoS_2 is expected to exhibit a reasonable response to electron acceptors.

To investigate the semiconducting behavior and sensing capabilities of MoS_2 materials, sensing experiments were conducted targeting NO_2 gas at a concentration of 20 ppm. In which, the sensor response was calculated using the following equation:

$$\frac{\Delta G}{G_o} = \left(\frac{G - G_o}{G_o}\right) \quad (1)$$

where G_0 and G are the electrical resistance values of the sensor device before and during exposure to NO_2 gas in a nitrogen environment, respectively. As shown in Figure 4, it can be observed that the resistance of MoS_2 nanosheets increased for all of the materials upon NO_2 exposure. NO_2 gas molecules are known for their electron-withdrawing characteristics due to the existence of a lone electron on the N atom.[12,13] Therefore, NO_2 molecules adsorbed on the MoS_2 surface cause a depletion of electrons in MoS_2, resulting in a decrease in the conductance or an increase in the resistance. These results provided solid evidence of the n-type behavior of MoS_2 because p-type MoS_2 materials induce resistance changes in the opposite direction, decreasing resistance, upon exposure to electron acceptors like NO_2 gas. This also confirmed that S vacancies are the dominant forms in MoS_2 since Mo vacancies induce p-type properties in MoS_2 materials.[37] Each increment in proton density induced a stronger response in resistance, as indicated, from the nonirradiated to the MoS_2 irradiated by the proton flux of 10^{14} ions/cm^2. The sensor response was nearly four-fold increased, with the highest responses reaching approximately 150%. These results were attributed to the intensification of S vacancies caused by elevated proton irradiation, as discussed above. Moreover, the induced vacancies in S, resulting from irradiation, appear to reach saturation after exposure to a proton flux of 1×10^{14} ions/cm^2. Increasing the proton density yields similar responses, plateauing, as illustrated in Figure 4b. Furthermore, the MoS_2-based sensors were subjected to a continuous series of NO_2 exposures at various concentrations. Each pulse, including supplying and evacuating a specific amount of NO_2, was well-controlled by a mass controller. As shown in Figure 5, the i10^{14}-based sensor was responsive to NO_2 concentrations, at a concentration range from 1 to 20 ppm, the sensor exhibited good linearity with a slope of 0.064 and r^2 = 0.9792. Because there was no discernible response obtained below a concentration of 1 ppm of NO_2, the lower limit of detection was taken to be 1 ppm, and the sensitivity was determined to be 28%/ppm. Interestingly, the sensors were exposed to a

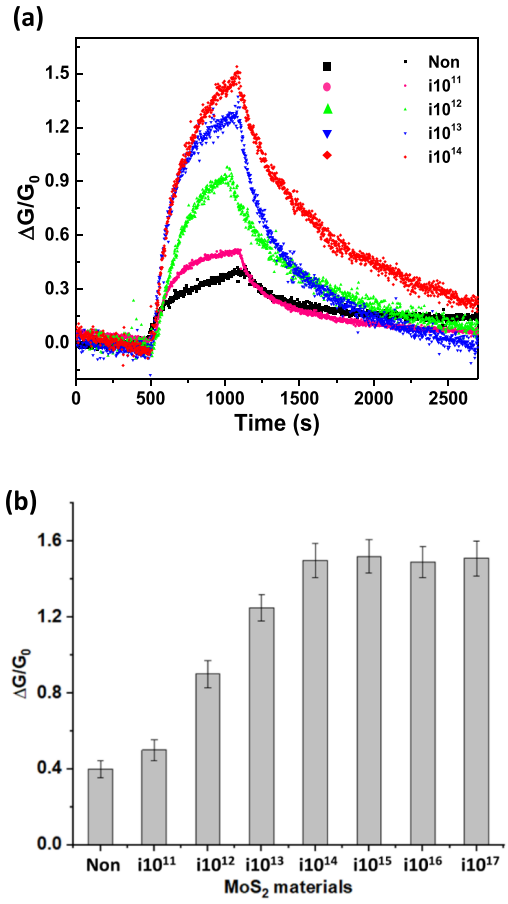

Figure 4. Sensor responses of nanosheets MoS_2 prepared from different fluxes of proton irradiation for NO_2 gas at concentration of 20 ppm; (a) real time responses and (b) responses with standard deviation.

sustained concentration of 10 ppm with 5 pulses, and the sensing signals were perfectly reproduced shortly after the application of the next NO_2 stream (Figure 5b). In addition, the sensor was exposed to different types of gas analytes, including NH_3, ethanol, acetone, and H_2O. As shown in Figure 6, in comparison to NO_2 sensing, the sensor exhibited responses in opposite directions because gas exposure led to a decrease in the resistance of the MoS_2 material, which is attributable to the electron-donating nature of these gases. It was evident that the sensor response to these interfering gases was negligible compared to that of NO_2. Considering the common presence of such gases in the atmosphere, the sensor was demonstrated to be reliable with high potential for real-world applications.

4. CONCLUSIONS

In this study, MoS_2 nanosheets with 2D layers of 4 nm thickness were successfully prepared from bulk MoS_2 by using ultrasonics. The MoS_2 treated with proton fluxes at a density of 1×10^{14} ions/cm^2 showed a high degree of S-vacancies. This was systematically demonstrated by red-shifted Raman spectra of E^1_{2g} and A_{1g} vibration modes and changes in the stoichiometric ratio between S and Mo atoms, which were obtained from the determination of binding energies for Mo 3d and S 2p orbitals. The NO_2 sensing performance of MoS_2 was proportionally improved with the density of proton irradiation, and the i10^{14}-based sensor exhibited the highest

https://doi.org/10.1021/acsomega.4c00379
ACS Omega 2024, 9, 27065−27070

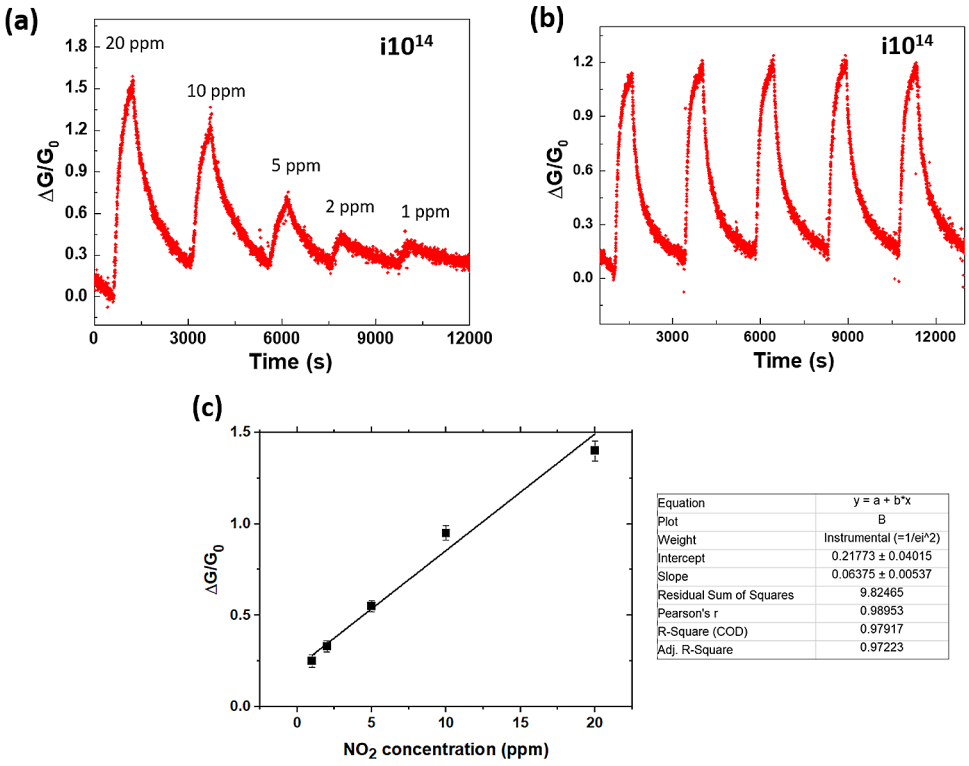

Figure 5. Sensing performance of the i10^{14}-irradiated MoS_2-based sensors for NO_2 gas; (a) sensor responses at a series of different NO_2 concentrations; (b) cycles of sensors responses at NO_2 concentrations of 10 ppm; (c) dependency of sensor responses on NO_2 concentrations ranging from 1 to 20 ppm.

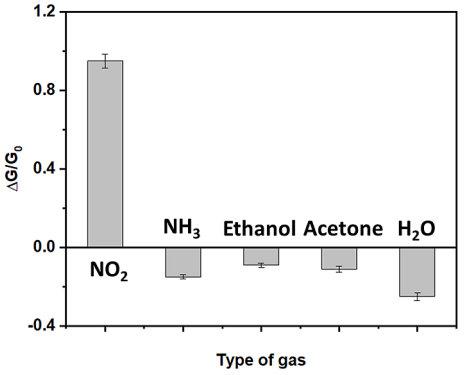

Figure 6. Sensor responses of the i10^{14}-irradiated MoS_2 with different gas analytes at a concentration of 10 ppm.

response to NO_2, with a response of 150% at 500 ppm. Proton irradiation was demonstrated to be effective in altering the chemical structures in MoS_2, with the aim to improve sensing capabilities. This approach shows high potential for other 2D materials.

■ ASSOCIATED CONTENT

Supporting Information

The Supporting Information is available free of charge at https://pubs.acs.org/doi/10.1021/acsomega.4c00379.

Histograms of exfoliated MoS_2 nanosheets (PDF)

■ AUTHOR INFORMATION

Corresponding Author

Nguyen Huu Hieu − *VNU-HCM Key Laboratory of Chemical Engineering and Petroleum Processing (Key CEPP Lab) and Faculty of Chemical Engineering, Ho Chi Minh City University of Technology (HCMUT), Ho Chi Minh City 70000, Vietnam; Vietnam National University Ho Chi Minh City (VNU-HCM), Ho Chi Minh City 71300, Vietnam;* orcid.org/0000-0003-1776-9871; Email: nhhieubk@hcmut.edu.vn

Authors

Ly Tan Nhiem − *Faculty of Chemical and Food Technology, Ho Chi Minh City University of Technology and Education, Ho Chi Minh City 71300, Vietnam;* orcid.org/0000-0003-4775-6174

Do Thuy Khanh Linh − *Faculty of Chemical and Food Technology, Ho Chi Minh City University of Technology and Education, Ho Chi Minh City 71300, Vietnam*

Hang Nguyen − *Development Group, Samsung Display Vietnam Co., Ltd., Yen Phong District, Bac Ninh Province 00700, Vietnam*

Complete contact information is available at: https://pubs.acs.org/10.1021/acsomega.4c00379

Notes

The authors declare no competing financial interest.

■ ACKNOWLEDGMENTS

This study is funded by the Ho Chi Minh City University of Technology and Education with the reference number T2023-23.

■ REFERENCES

(1) Yang, T.; Song, T. T.; Zhou, J.; Wang, S.; Chi, D.; Shen, L.; Yang, M.; Feng, Y. P. High-Throughput Screening of Transition Metal

Single Atom Catalysts Anchored on Molybdenum Disulfide for Nitrogen Fixation. *Nano Energy* **2020**, *68*, No. 104304.
(2) Gupta, D.; Chauhan, V.; Kumar, R. A Comprehensive Review on Synthesis and Applications of Molybdenum Disulfide (MoS2) Material: Past and Recent Developments. *Inorg. Chem. Commun.* **2020**, *121*, No. 108200.
(3) Huang, Y.; Yu, K.; Li, H.; Xu, K.; Liang, Z.; Walker, D.; Ferreira, P.; Fischer, P.; Fan, D. E. Scalable Fabrication of Molybdenum Disulfide Nanostructures and Their Assembly. *Adv. Mater.* **2020**, *32* (43), No. 2003439.
(4) Imani Yengejeh, S.; Liu, J.; Kazemi, S. A.; Wen, W.; Wang, Y. Effect of Structural Phases on Mechanical Properties of Molybdenum Disulfide. *ACS Omega* **2020**, *5* (11), 5994−6002.
(5) Zribi, R.; Neri, G. Mo-Based Layered Nanostructures for the Electrochemical Sensing of Biomolecules. *Sensors* **2020**, *20* (18), 5404.
(6) Rawat, A.; Mohanta, M. K.; Jena, N.; Dimple; Ahammed, R.; De Sarkar, A. Nanoscale Interfaces of Janus Monolayers of Transition Metal Dichalcogenides for 2D Photovoltaic and Piezoelectric Applications. *J. Phys. Chem. C* **2020**, *124* (19), 10385−10397.
(7) Tian, Y.; Zeng, G.; Rutt, A.; Shi, T.; Kim, H.; Wang, J.; Koettgen, J.; Sun, Y.; Ouyang, B.; Chen, T.; Lun, Z.; Rong, Z.; Persson, K.; Ceder, G. Promises and Challenges of Next-Generation "Beyond Li-Ion" Batteries for Electric Vehicles and Grid Decarbonization. *Chem. Rev.* **2021**, *121* (3), 1623−1669.
(8) Lin, D.; Rangarajan, S. A DFT Study of Site-Dependent Energetics of Hexagonal MoS2 Nanoparticles under Varying Reaction Conditions. *Surf. Sci.* **2023**, *729*, No. 122231.
(9) Kumar, R.; Zheng, W.; Liu, X.; Zhang, J.; Kumar, M. MoS2-Based Nanomaterials for Room-Temperature Gas Sensors. *Advanced Materials Technologies* **2020**, *5* (5), 1901062.
(10) Liu, B.; Chen, L.; Liu, G.; Abbas, A. N.; Fathi, M.; Zhou, C. High-Performance Chemical Sensing Using Schottky-Contacted Chemical Vapor Deposition Grown Monolayer MoS2 Transistors. *ACS Nano* **2014**, *8* (5), 5304−5314.
(11) Late, D. J.; Huang, Y.-K.; Liu, B.; Acharya, J.; Shirodkar, S. N.; Luo, J.; Yan, A.; Charles, D.; Waghmare, U. V.; Dravid, V. P.; Rao, C. N. R. Sensing Behavior of Atomically Thin-Layered MoS2 Transistors. *ACS Nano* **2013**, *7* (6), 4879−4891.
(12) Thi Mong Thy, L.; Tien Giang, N.; Hang, N.; Tan Nhiem, L. Defect Engineering of CVD Graphene and Real-Time Raman Study of NO2 Adsorption toward Enhanced Sensing Sensitivity. *FlatChem.* **2023**, *39*, No. 100505.
(13) Hang, N.; Hieu, N. H.; Nhiem, L. T. Sensitive NO2 Sensor Based on Silver Nanowires-Decorated Monolayer Graphene with Assistance of UV Illumination. *J. Mater. Sci: Mater. Electron* **2023**, *34* (2), 90.
(14) Korotcenkov, G.; Brinzari, V.; Cho, B. K. Conductometric Gas Sensors Based on Metal Oxides Modified with Gold Nanoparticles: A Review. *Microchim Acta* **2016**, *183* (3), 1033−1054.
(15) Ly, T. N.; Park, S. Highly Sensitive Ammonia Sensor for Diagnostic Purpose Using Reduced Graphene Oxide and Conductive Polymer. *Sci. Rep* **2018**, *8* (1), 18030.
(16) Ly, T. N.; Park, S. Highly Sensitive Gas Sensor Using Hierarchically Self-Assembled Thin Films of Graphene Oxide and Gold Nanoparticles. *Journal of Industrial and Engineering Chemistry* **2018**, *67*, 417−428.
(17) Do, M. H.; Nhiem, L. T. Multifunctional Sensor Based on Hybrid Material of Reduced Graphene Oxide and Polyaniline. *J. Electron. Mater.* **2023**, *52* (6), 4037−4044.
(18) van der Zande, A. M.; Huang, P. Y.; Chenet, D. A.; Berkelbach, T. C.; You, Y.; Lee, G.-H.; Heinz, T. F.; Reichman, D. R.; Muller, D. A.; Hone, J. C. Grains and Grain Boundaries in Highly Crystalline Monolayer Molybdenum Disulphide. *Nat. Mater.* **2013**, *12* (6), 554−561.
(19) Li, Y.; Song, Z.; Li, Y.; Chen, S.; Li, S.; Li, Y.; Wang, H.; Wang, Z. Hierarchical Hollow MoS2Microspheres as Materials for Conductometric NO2 Gas Sensors. *Sens. Actuators, B* **2019**, *282*, 259−267.
(20) Kim, S.; Han, J.; Kang, M.-A.; Song, W.; Myung, S.; Kim, S.-W.; Lee, S. S.; Lim, J.; An, K.-S. Flexible Chemical Sensors Based on Hybrid Layer Consisting of Molybdenum Disulphide Nanosheets and Carbon Nanotubes. *Carbon* **2018**, *129*, 607−612.
(21) Cho, B.; Yoon, J.; Lim, S. K.; Kim, A. R.; Kim, D.-H.; Park, S.-G.; Kwon, J.-D.; Lee, Y.-J.; Lee, K.-H.; Lee, B. H.; Ko, H. C.; Hahm, M. G. Chemical Sensing of 2D Graphene/MoS2 Heterostructure Device. *ACS Appl. Mater. Interfaces* **2015**, *7* (30), 16775−16780.
(22) Liu, A.; Lv, S.; Jiang, L.; Liu, F.; Zhao, L.; Wang, J.; Hu, X.; Yang, Z.; He, J.; Wang, C.; Yan, X.; Sun, P.; Shimanoe, K.; Lu, G. The Gas Sensor Utilizing Polyaniline/MoS2 Nanosheets/SnO2 Nanotubes for the Room Temperature Detection of Ammonia. *Sens. Actuators, B* **2021**, *332*, No. 129444.
(23) Cho, S.-Y.; Koh, H.-J.; Yoo, H.-W.; Kim, J.-S.; Jung, H.-T. Tunable Volatile-Organic-Compound Sensor by Using Au Nanoparticle Incorporation on MoS2. *ACS Sens.* **2017**, *2* (1), 183−189.
(24) Kwon, S.; Choi, S. H.; Kim, Y. J.; Yoon, I. T.; Yang, W. Proton Beam Flux Dependent Work Function of Mono-Layer MoS2. *Thin Solid Films* **2018**, *660*, 766−770.
(25) Kim, T.-Y.; Cho, K.; Park, W.; Park, J.; Song, Y.; Hong, S.; Hong, W.-K.; Lee, T. Irradiation Effects of High-Energy Proton Beams on MoS2 Field Effect Transistors. *ACS Nano* **2014**, *8* (3), 2774−2781.
(26) Gupta, A.; Arunachalam, V.; Vasudevan, S. Water Dispersible, Positively and Negatively Charged MoS2 Nanosheets: Surface Chemistry and the Role of Surfactant Binding. *J. Phys. Chem. Lett.* **2015**, *6* (4), 739−744.
(27) Ganatra, R.; Zhang, Q. Few-Layer MoS2: A Promising Layered Semiconductor. *ACS Nano* **2014**, *8* (5), 4074−4099.
(28) Nam, G.-H.; He, Q.; Wang, X.; Yu, Y.; Chen, J.; Zhang, K.; Yang, Z.; Hu, D.; Lai, Z.; Li, B.; Xiong, Q.; Zhang, Q.; Gu, L.; Zhang, H. In-Plane Anisotropic Properties of 1T′-MoS2 Layers. *Adv. Mater.* **2019**, *31* (21), 1807764.
(29) Li, H.; Zhang, Q.; Yap, C. C. R.; Tay, B. K.; Edwin, T. H. T.; Olivier, A.; Baillargeat, D. From Bulk to Monolayer MoS2: Evolution of Raman Scattering. *Adv. Funct. Mater.* **2012**, *22* (7), 1385−1390.
(30) Dash, A. K.; Swaminathan, H.; Berger, E.; Mondal, M.; Lehenkari, T.; Prasad, P. R.; Watanabe, K.; Taniguchi, T.; Komsa, H.-P.; Singh, A. Controlled Defect Production in Monolayer MoS2 via Electron Irradiation at Ultralow Accelerating Voltages. *2D Mater.* **2023**, *10* (3), No. 035002.
(31) Qin, S.; Lei, W.; Liu, D.; Chen, Y. In-Situ and Tunable Nitrogen-Doping of MoS2 Nanosheets. *Sci. Rep* **2014**, *4* (1), 7582.
(32) Vancsó, P.; Magda, G. Z.; Pető, J.; Noh, J.-Y.; Kim, Y.-S.; Hwang, C.; Biró, L. P.; Tapasztó, L. The Intrinsic Defect Structure of Exfoliated MoS2 Single Layers Revealed by Scanning Tunneling Microscopy. *Sci. Rep* **2016**, *6* (1), 29726.
(33) McDonnell, S.; Addou, R.; Buie, C.; Wallace, R. M.; Hinkle, C. L. Defect-Dominated Doping and Contact Resistance in MoS2. *ACS Nano* **2014**, *8* (3), 2880−2888.
(34) Baker, M. A.; Gilmore, R.; Lenardi, C.; Gissler, W. XPS Investigation of Preferential Sputtering of S from MoS2 and Determination of MoSx Stoichiometry from Mo and S Peak Positions. *Appl. Surf. Sci.* **1999**, *150* (1), 255−262.
(35) Kondekar, N. P.; Boebinger, M. G.; Woods, E. V.; McDowell, M. T. In Situ XPS Investigation of Transformations at Crystallographically Oriented MoS2 Interfaces. *ACS Appl. Mater. Interfaces* **2017**, *9* (37), 32394−32404.
(36) Baugher, B. W. H.; Churchill, H. O. H.; Yang, Y.; Jarillo-Herrero, P. Intrinsic Electronic Transport Properties of High-Quality Monolayer and Bilayer MoS2. *Nano Lett.* **2013**, *13* (9), 4212−4216.
(37) Salehi, S.; Saffarzadeh, A. Atomic Defect States in Monolayers of MoS2 and WS2. *Surf. Sci.* **2016**, *651*, 215−221.

https://doi.org/10.1021/acsomega.4c00379
ACS Omega 2024, 9, 27065−27070